

Supplementary Materials for

Mediobasal hypothalamic FKBP51 acts as a molecular switch linking autophagy to whole-body metabolism

Alexander S. Häusl*, Thomas Bajaj*, Lea M. Brix, Max L. Pöhlmann, Kathrin Hafner, Meri De Angelis, Joachim Nagler, Frederik Dethloff, Georgia Balsevich, Karl-Werner Schramm, Patrick Giavalisco, Alon Chen, Mathias V. Schmidt, Nils C. Gassen

*Corresponding author. Email: mschmidt@psych.mpg.de (M.V.S.); nils.gassen@ukbonn.de (N.C.G.)

Published 9 March 2022, *Sci. Adv.* **8**, eabi4797 (2022)

DOI: 10.1126/sciadv.abi4797

The PDF file includes:

Figs. S1 to S10

Other Supplementary Material for this manuscript includes the following:

Data S1

Supplementary figure 1: FKBP51 deletion alters AMPK and mTOR-associated amino acid metabolic and biosynthetic pathways.

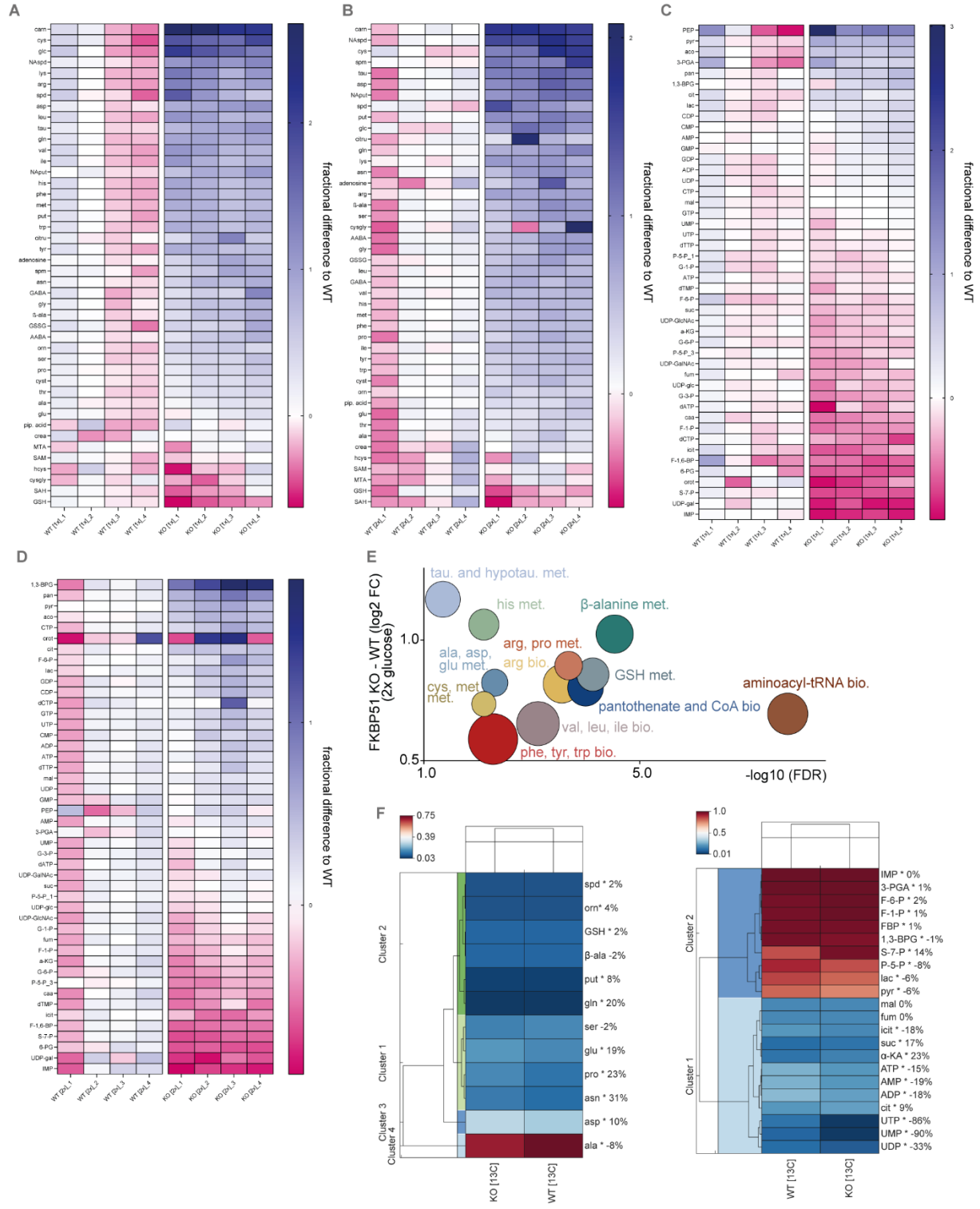


Fig. S1: FKBP51 deletion alters AMPK and mTOR-associated amino acid metabolic and biosynthetic pathways. **(A)** Heatmap of altered amine-containing (Bz) metabolites in SH-SY5Y cells lacking FKBP51 and WT control cells cultured under normal glucose condition (1x, 4.5 g/l) and **(B)** increased glucose condition (2x, 9 g/l). **(C)** Heatmaps of altered anionic (IC) metabolites in SH-SY5Y cells lacking FKBP51 compared to WT control cells under normal and **(D)** increased glucose culturing conditions. The fractional differences of each replicate are shown for all metabolites comparing the genotype and the different glucose conditions. **(E)** Analysis and regulation of significantly altered pathways of FKBP51 KO and WT cells under excessive glucose conditions. The f(x)-axis shows the (median) log₂ fold change (FC) of all significantly altered metabolites of the indicated pathway and the false discovery rate (FDR, equals the $-\log_{10}$ adjusted p-value) is shown on the x-axis. The size of the circles represents the amount of significantly changed metabolites in comparison to all metabolites of a particular pathway. **(F)** Analysis of the metabolic flux in FKBP51 KO cells compared to WT cells using C¹³ glucose as tracer. The enrichment of C¹³ is displayed for each metabolite investigated.

Fig. S2: FKBP51 deletion alters AMPK and mTOR-associated amino acid metabolic and biosynthetic pathways in murine neuroblastoma cells.

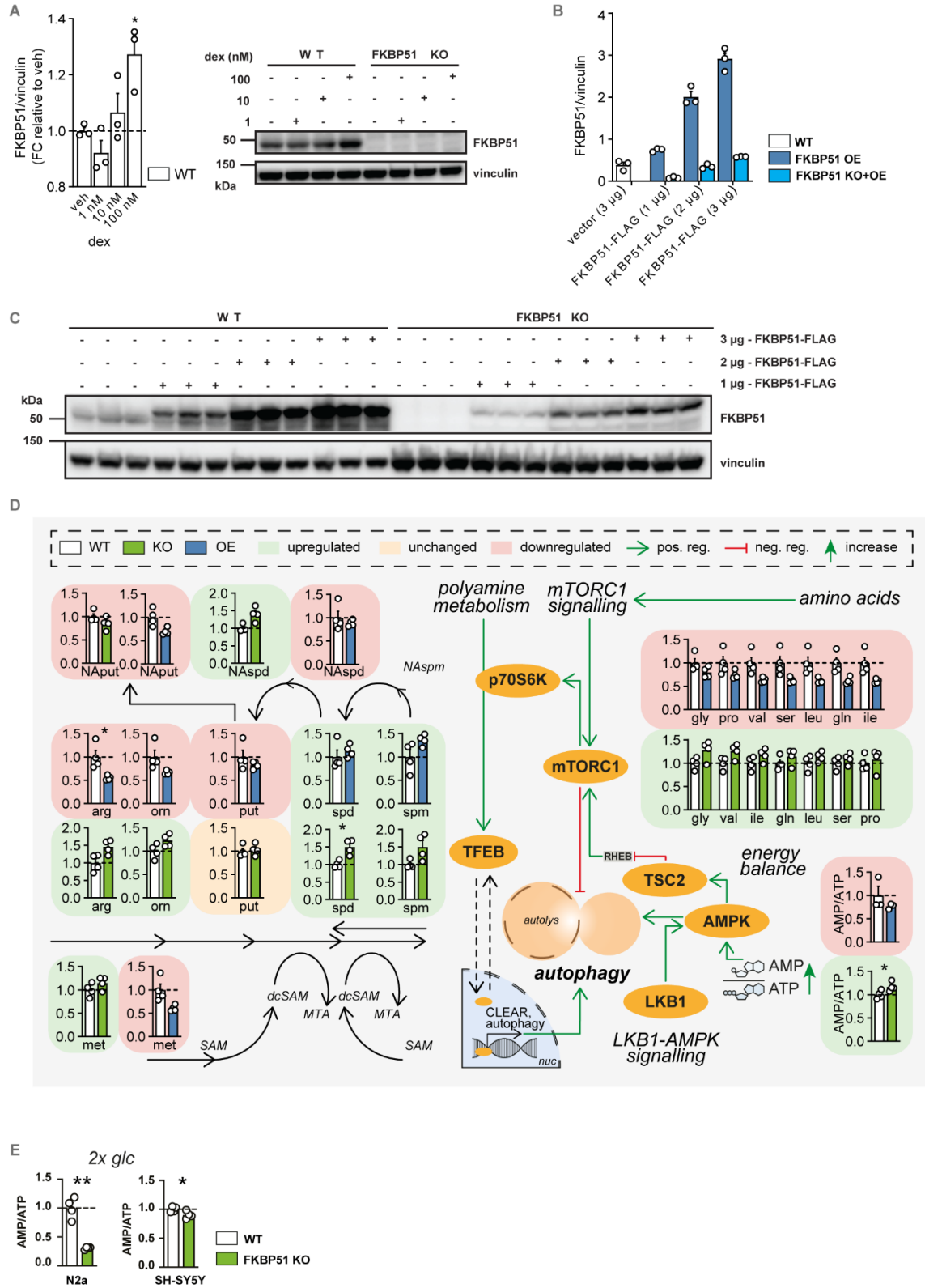


Fig. S2: FKBP51 deletion alters AMPK and mTOR- associated amino acid metabolic and biosynthetic pathways in murine neuroblastoma cells. (A, B) Validation of FKBP51 responsiveness in WT N2a cells to dexamethasone stimulation. (C) Titration of FKBP51-FLAG expression construct in FKBP51 WT and KO N2a cells (n=3). (D) FKBP51 deletion and overexpression (OE) in N2a cells alters metabolites of the polyamine pathway and levels of amino acids associated with mTOR signaling. (E) AMP/ATP ratio in N2a and SH-SY5Y FKBP51 KO cells under increased glucose conditions. All data are shown as relative fold change compared to control condition; \pm s.e.m.; One-way ANOVA followed by Dunnett's multiple comparison test for A, the paired student's t-test was performed in D and E. * $p < 0.05$, ** $p < 0.01$, * $p < 0.001$;**

Abbreviations: AMP, adenosine monophosphate; AMPK, AMP-activated protein kinase; arg, arginine; ATP, adenosine triphosphate; dex, dexamethasone; dcSAM, decarboxylated S-adenosylmethione; glc, glucose; gln, glutamine; gly, glycine; ile, isoleucine; leu, leucine; LKB1, liver kinase B 1; met, methionine; MTA, 5'-methylthioadenosine; mTORC1, mechanistic target of rapamycin complex 1; NAput, N-acetylputrescine; NAspd, N-acetylspermidine; NAspm, N-acetylspermine; orn, ornithine pro; proline; put, putrescine; SAM, S-adenosylmethionine; ser, serine; spd, spermidine; spm, spermine; TFEB, transcription factor EB; TSC2, tuberous sclerosis complex 2; val, valine; veh, vehicle.

presence or absence of BafA1 to assess autophagy flux (**I**). Representative blots of autophagy flux assay. All data are shown as relative fold change compared to control condition; \pm s.e.m.; a two-way ANOVA was performed in (**A-C**) and followed by a Tukey's multiple comparison test. One-way ANOVA followed by a Dunnett's multiple comparison test was performed for (**I**). The unpaired student's t-test was performed in (**D-L**). * $p < 0.05$, ** $p < 0.01$, *** $p < 0.001$; # $p < 0.05$, ## $p < 0.01$. * = significant genotype effect; # = significant treatment effect.

Fig. S4: FKBP51 does not alter hypusination of eIF5A.

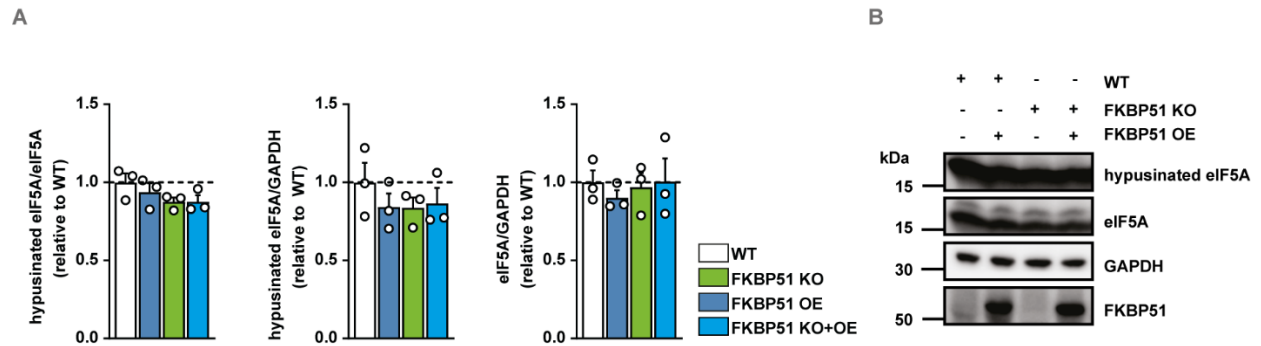


Fig. S4: FKBP51 does not alter hypusination of eIF5A.

(A) Hypusination of eIF5A is not affected by FKBP51 KO or expression level in N2a cells.

(B) Representative blots of hypusinated eIF5A, total eIF5A, GAPDH and FKBP51.

Fig. S5: *In-vitro* manipulation of FKBP51 and its effects on autophagy signaling.

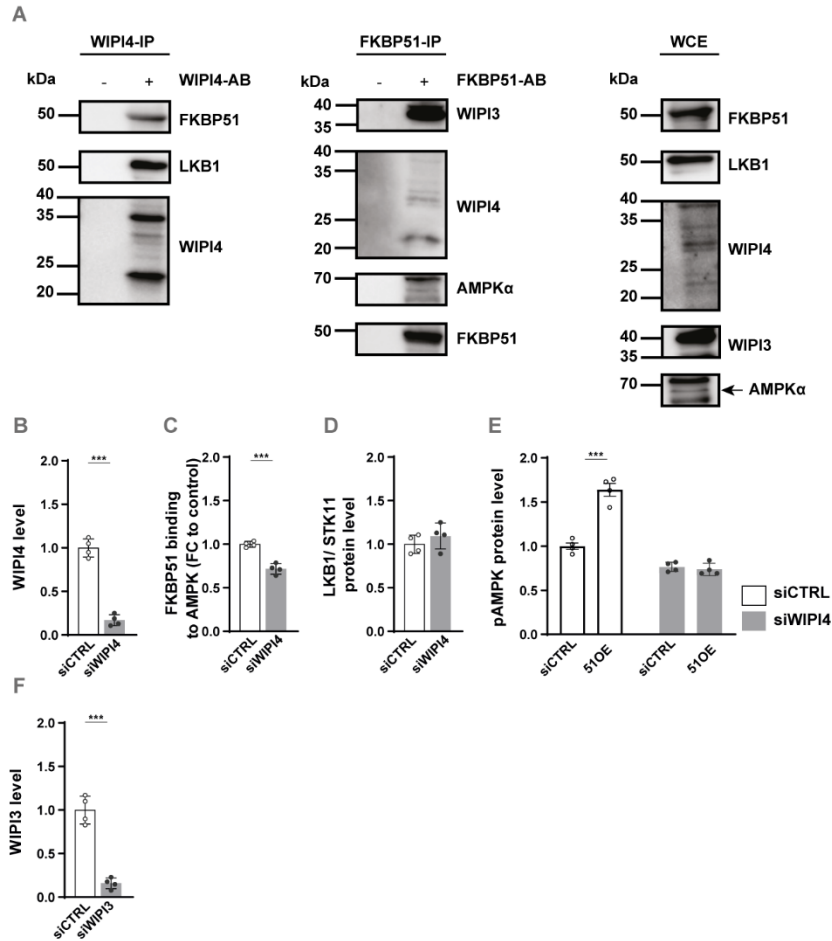


Fig. S5: FKBP51 associates with AMPK, TSC2, and WIPI3 & 4 to regulate autophagy and mTOR signaling. (A) Endogenously expressed FKBP51 associates with WIPI4, LKB1, WIPI3 and AMPK α in WT N2a cells. **(B)** Confirmation of WIPI4 KD in N2a cells. **(C)** FKBP51 binding to AMPK α 1 in WIPI4 KD cells. **(D)** LKB1 binding to FKBP51 was not affected in WIPI4-KD cells. **(E)** WIPI4 KD blocked the FKBP51 overexpressing (51OE) effect on pAMPK at T172 **(F)** WIPI3 KD in N2a cells. All data are shown as relative fold change compared to control condition and were analyzed with an unpaired t-test; \pm SEM; * $p < 0.05$, ** $p < 0.01$, *** $p < 0.001$.

Fig. S6: FKBP51 overexpression in the MBH affects sympathetic outflow to muscle and fat tissue.

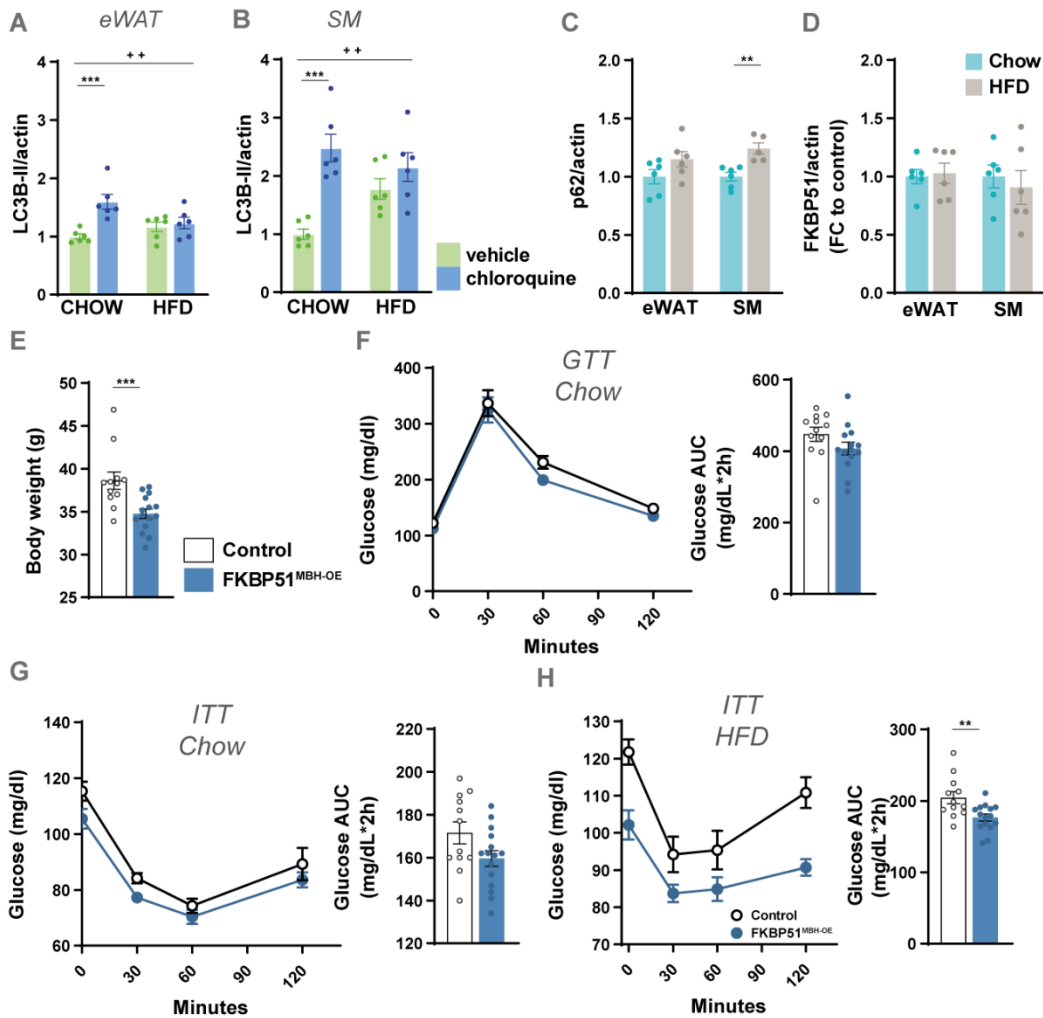


Fig. S6: FKBP51 overexpression in the MBH affects sympathetic outflow to muscle and fat tissue. (A) LC3B-II levels before and after chloroquine treatment (50 mg/kg) in eWAT and (B) soleus muscle under chow and HFD conditions (C) 10 weeks of HFD increased the accumulation of the autophagy receptor p62 in SM, but not in eWAT. (D) FKBP51 expression in soleus muscle (SM) and epididymal white adipose tissue (eWAT) after 10 weeks of HFD. (E) Overexpression of FKBP51 in a second cohort of C57/B16 animals resulted in a lean body weight phenotype after 10 weeks of HFD. (F-H) Differences in glucose metabolism were investigated by performing a

glucose tolerance test (GTT) and an insulin tolerance test (ITT) under chow and HFD conditions. For **(A, B)** a two-way ANOVA was performed followed by a Tukey's multiple comparisons test and data are shown as relative fold change compared to control condition. For **(C - H)** an unpaired student's t-test was performed. \pm SEM; * $p < 0.05$, ** $p < 0.01$, *** $p < 0.001$; + $p < 0.05$, ++ $p < 0.01$. * = significant treatment effect; + = significant treatment x diet interaction.

Fig. S7: FKBP51 regulates autophagy signaling in the MBH.

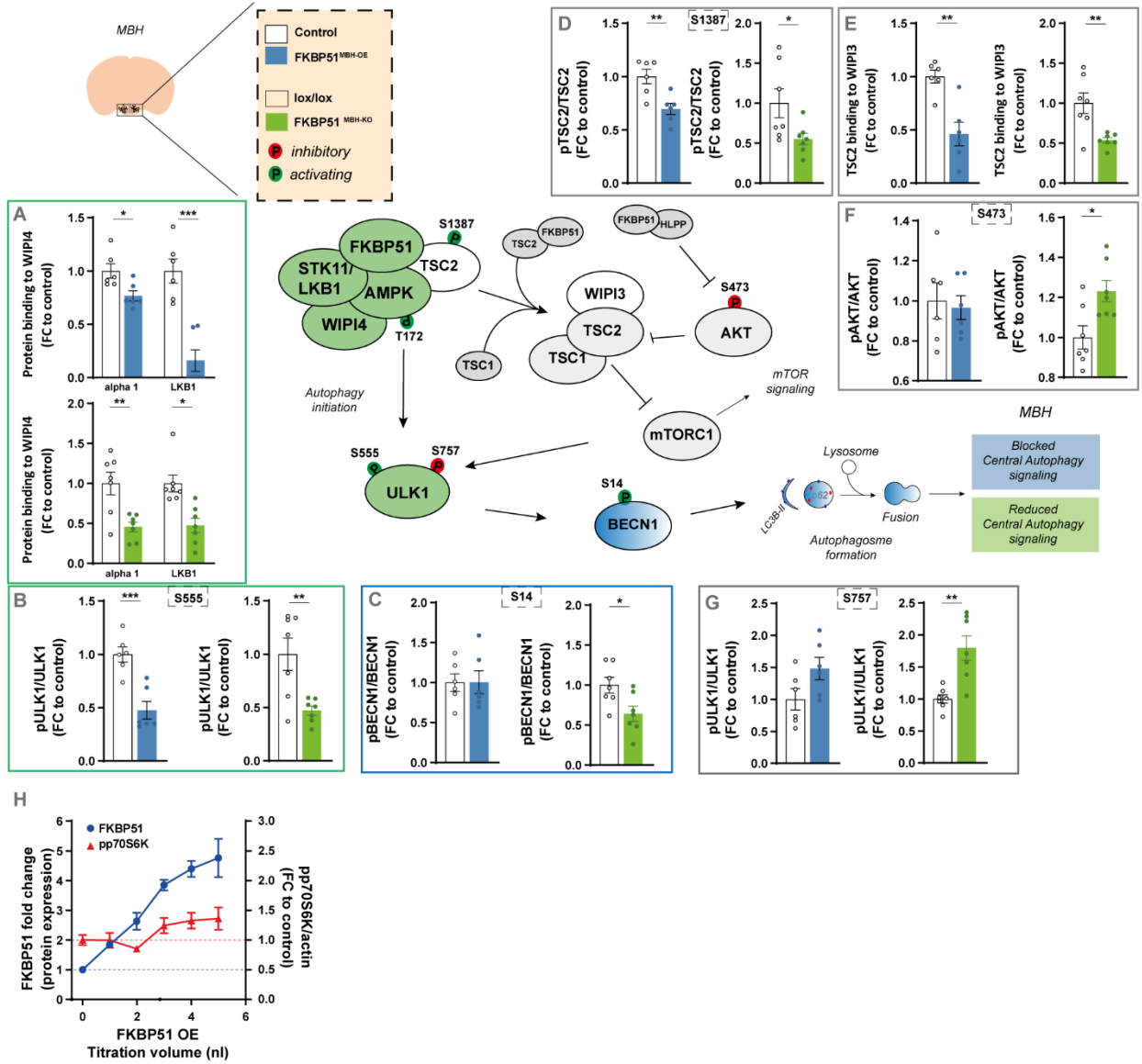


Fig. S7: FKBP51 regulates autophagy signaling in the MBH. Pathway analysis of main autophagy and mTOR regulators in the mediobasal hypothalamus (MBH). FKBP51 overexpression is depicted in blue and FKBP51 deletion is depicted in green. (A) Quantification of LKB1 and AMPK binding to WIPI4. (B) Phosphorylation of ULK1 at S555, (C) pBECN1 at S14, (D) pTSC2 at S1387. (E) Quantification of TSC2 binding to WIPI3. (F) Phosphorylation of AKT at S473, and (G) ULK1 at S757. (H) Quantification of pp70S6K while titrating AAV-HA-

FKBP51 virus into N2a cells. All data are shown as relative fold change compared to control condition and were analyzed with an unpaired t-test.; \pm SEM; * $p < 0.05$, ** $p < 0.01$, *** $p < 0.001$.

Fig. S8: Effects of hypothalamic FKBP51 overexpression on peripheral autophagy signaling.

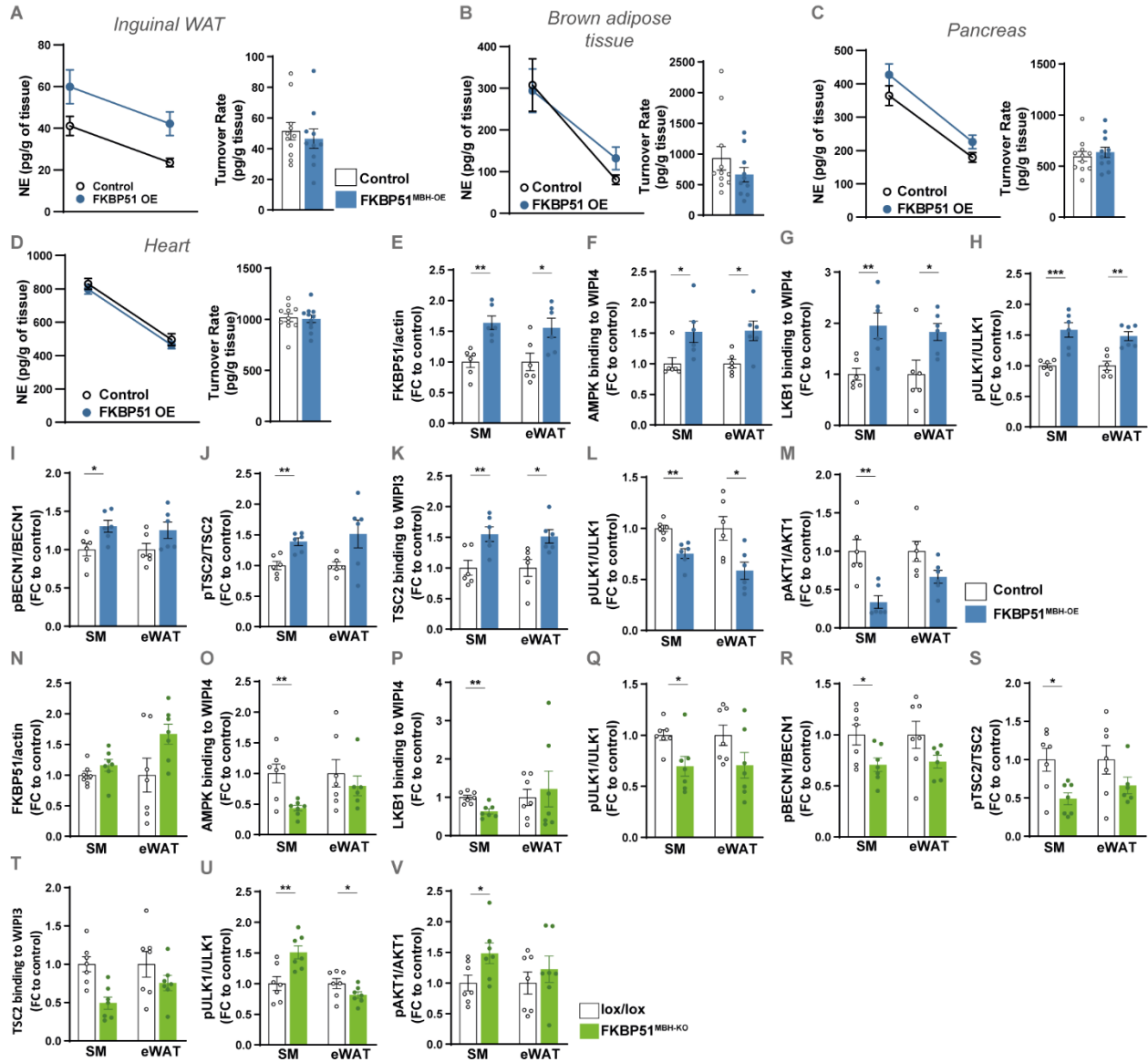


Fig. S8: Effects of hypothalamic FKBP51 overexpression on peripheral autophagy signaling.

(A-D) Representative decrease in tissue NE content after MPT injection (left panel) and turnover rate (right panel) were determined on inguinal WAT and brown adipose tissue (BAT), pancreas, and heart. (E-V) Pathway analysis of main autophagy and mTOR marker in the soleus muscle (SM) and epididymal white adipose tissue (eWAT). FKBP51 overexpression is depicted in blue and FKBP51 deletion is depicted in green. (E) Quantification of FKBP51 protein level. (F)

Quantification of AMPK and (G) LKB1 binding to WIPI4. (H) Phosphorylation of ULK1 at S555, (I) pBECN1 at S14, (J) TSC2 at S1387. (K) Quantification of TSC2 binding to WIPI3. (L) Phosphorylation of ULK1 at S757, and (M) AKT1 at S473. (N) FKBP51 level in SM and eWAT of FKBP51^{MBH-KO} mice. (O) Quantification of AMPK and (P) LKB1 binding to WIPI4. (Q) Phosphorylation of ULK1 at S555, (R) pBECN1 at S14, (S) TSC2 at S1387. (T) Quantification of TSC2 binding to WIPI3. (U) Phosphorylation of ULK1 at S757, and (V) AKT1 at S473. All data are shown as relative fold change compared to control condition and were analyzed with an unpaired t-test.; ± SEM; * p < 0.05, **p < 0.01, ***p < 0.001.

Fig. S9: AMPK and mTOR signaling was not affected in in liver tissue of FKBP51^{MBH-KO} mice.

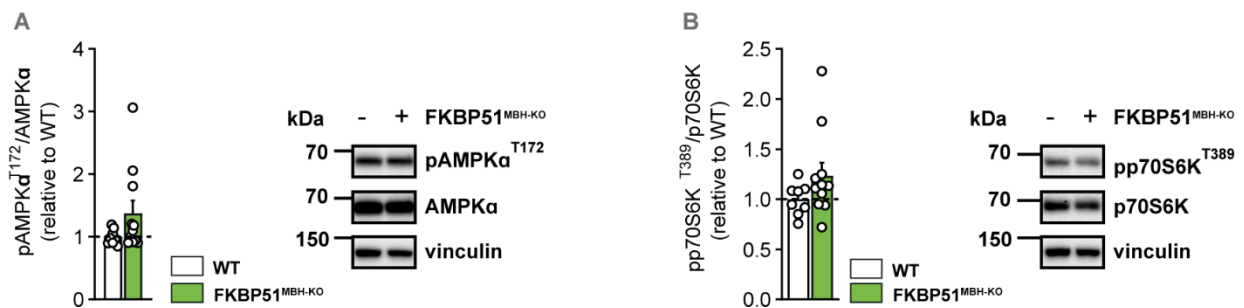


Fig. S9: AMPK and mTOR signaling was not affected in liver tissue of FKBP51^{MBH-KO} mice.

(A) Representative blots and quantification of AMPK phosphorylation at T172 and (B) p70S6K in liver tissue of FKBP51^{MBH-KO} mice (n = 8 for WT, n = 11 for KO). All data are shown as relative fold change compared to control condition and were analyzed with an unpaired t-test.; ± SEM; * p < 0.05, **p < 0.01, ***p < 0.001.

Fig. S10:

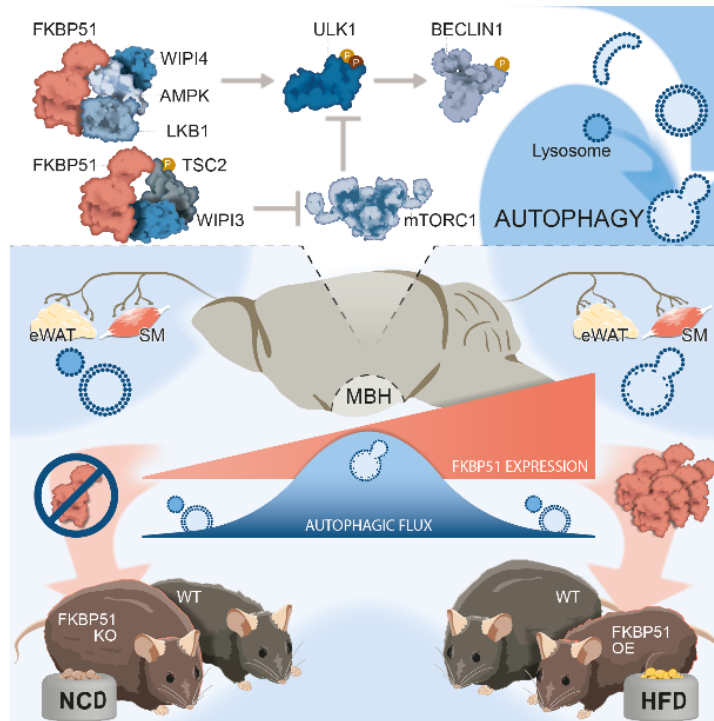


Fig. S10: The stress-responsive FKBP51 controls body weight gain by regulating the balance between autophagy and mTOR signaling. We identified FKBP51 as a central nexus for the recruitment of the LKB1/AMPK complex to WIPI4 and TSC2 to WIPI3, thereby regulating the balance between autophagy and mTOR signaling in response to metabolic challenges. MBH FKBP51 dose-dependently regulates autophagy both in the brain as well as in peripheral metabolic tissues. Consequently, deletion of MBH FKBP51 strongly induces obesity, while its overexpression protects against high-fat diet (HFD) induced obesity.